Editors' Suggestion

Predicting failure locations in model end-linked polymer networks

Han Zhang (张菡) and Robert A. Riggleman*
Department of Chemical and Biomolecular Engineering, University of Pennsylvania, Philadelphia, Pennsylvania 19104, USA

(Received 16 October 2023; accepted 26 February 2024; published 27 March 2024)

The fracture of polymer networks and gels has a significant impact on the performance of these versatile and widely used materials, and a molecular-level understanding of the fracture process is crucial for the design of new materials. Combining molecular dynamics simulations and network analysis techniques, we demonstrate that in the initial undeformed state of model end-linked polymer networks, polymer strands with fewer topological defects in their local surroundings, higher geodesic edge betweenness centrality values compared to the system average, and greater alignment to the loading direction are more prone to breaking under uniaxial tensile deformation.

DOI: 10.1103/PhysRevMaterials.8.035604

I. INTRODUCTION

Polymer networks and gels are significant and highly versatile materials with their broad applications across diverse fields such as membranes, drug delivery systems, and soft electronic devices [1–7]. Given their wide-ranging use in people's daily lives, the fracture of these soft materials profoundly impacts their applications and performance. Understanding the fracture of polymer networks from a molecular perspective is crucial for advancing their utilization and facilitating the design of new materials [8–16].

Investigating the relationship between the macroscopic properties of polymer networks and their network structures and topology has been a challenging and long-standing problem in the fields of polymer physics and soft matter [17]. The properties of these soft amorphous materials depend on how molecules connect with each other in the networks, and the existence of topological defects, including loops and dangling ends, further complicates the understanding of these relationships. Over the last decade, the impact of topological defects on the polymer network elasticity [18–23] and fracture [10–13] has been incorporated into classic models [24,25], resulting in improved agreement with experimental results. Despite these advancements, the relationship between the fracture behavior and the molecular-level structures of polymer networks still remains elusive.

Network analysis has recently emerged as a novel approach for studying complex disordered systems [26–36]. Representing disordered particulate systems as network structures offers an approach to characterize those systems across multiple length scales. Among various metrics used to quantify the network structures, the geodesic edge betweenness centrality (GEBC) has proven to be particularly useful in predicting failure locations in various disordered systems [29,33,35,37]. GEBC, a specific type of betweenness centrality, measures the degree to which an edge lies on the shortest (geodesic) paths connecting nodes within the networks [26,38]. Berthier *et al.* demonstrated the effectiveness of GEBC in accessing possible failure locations in two-dimensional disordered lattices with structures constructed from contact networks in granular media [29]. Mangal *et al.* found that bonds with higher GEBC are more likely to rupture in short-ranged weakly attractive colloidal gels at different deformation rates [35]. These studies highlight the utility of the network analysis techniques, especially GEBC as a predictive tool for understanding the failure behavior of diverse disordered systems. While molecular simulations have become increasingly common tools to study polymer networks in recent years [12,13,20,39–48], there still exists a gap in our understanding between network topology and properties. Network analysis techniques offer a promising route to incorporate chain-level information to the existing polymer network models and therefore hold immense potential for unraveling the intricate interplay between their molecular structures and macroscopic behaviors.

In this paper, we combine molecular dynamics simulations and network analysis techniques to predict the local failure locations at the level of individual polymer strands in model end-linked polymer networks with topological defects. By analyzing the isoconfigurational ensemble with uniaxial tensile deformations, we find that the failure locations of polymer networks are influenced by the underlying network structure. We find that for polymer strands with high probabilities of breaking, their local environment contains fewer primary loop defects. The presence of the topological defects also leads to a nonuniform distribution of GEBC across polymer strands within the networks, enabling the prediction of failure locations. GEBC of each strand and the angle between the loading direction and each strand are calculated from the initial undeformed states of the networks. We find a positive correlation between GEBC and the probability of breaking of polymer strands and the strands that are more aligned with the loading direction have a higher probability of breaking. Moreover, strand breaking events initiate from polymer strands with high GEBC values and small angles between the strands and the loading direction. These findings provide an effective approach to identify potential failure locations within the polymer networks based solely on their initial undeformed

*rrig@seas.upenn.edu

configurations, offer a different perspective to understand the impact of topological defects in the networks and shed light on the inverse design strategies of network materials with desired fracture properties.

II. SIMULATION METHODS

We implement coarse-grained molecular dynamics (MD) simulations in the LAMMPS package [49,50] to generate end-linked polymer networks following our previous works [13,45]. All simulations are performed on Stampede2 from the Texas Advanced Computing Center (TACC) through the Advanced Cyberinfrastructure Coordination Ecosystem: Services and Support (ACCESS) program [51]. Our approach aims at mimicking experimental systems where linear polymer chains with reactive endgroups react with tetrafunctional crosslinkers [52], and previous comparisons of our simulations to experimental results show very good qualitative agreement in their properties [13]. We begin with a polymer melt of $2n$ identical monodispersed polymer chains with N monomers per chain and n crosslinkers that are chemically identical to the polymer monomers. In this paper, we study network systems with $N = 5$, 15, and 50. All crosslinkers and monomers are modeled as chemically identical Lennard-Jones beads. Bonding is maintained through a harmonic bond potential. The isothermal-isobaric ensemble is used to equilibrate the melt. We then allow the reactions to take place between the chain ends and the crosslinkers. The topological defects are naturally emergent from the reactive MD method [45]. After the network is formed and equilibrated, we modify the bonding interactions to the breakable quartic potential to allow chain scission for fracture studies.

The network is reequilibrated prior to deformation under the quartic bond potential. While performing the uniaxial tensile deformation, the simulation box is expanded uniaxially along an axis until all bonds lying along on a plane are broken. The pressure in the other two directions is kept constant while performing the deformation. Full simulation details, sample stress-strain curves, and key fracture properties are available in the Supplemental Material [53].

The effect of the network structure on the failure locations in polymer networks is investigated using the isoconfigurational ensemble [54,55]. Using the same network configuration, the velocities of all particles are reinitialized in each run prior to deformation. Uniaxial tensile deformations are then performed for all runs with the same direction and strain rate. The isoconfigurational ensemble approach enables us to determine whether the fracture process in polymer networks is purely stochastic or influenced by the underlying network structure. If the failure locations are not structure related, a random set of strands will break in each run. However, if the failure locations are structure related, there will be a significant overlap between the strands broken across multiple runs. When the entire plane of a network along the loading direction fractures, the molecular IDs of broken strands are recorded in each run. The probability of breaking P_{break} of each polymer strand i is defined as

$$P_{i,\text{break}} = \frac{n_{i,\text{break}}}{n_{\text{runs}}}, \tag{1}$$

where $n_{i,\text{break}}$ is the number of times strand i breaks in the isoconfigurational ensemble and $n_{\text{runs}} = 10$ for each configuration. For each configuration, the isoconfigurational ensemble is performed in all three directions to ensure that the results are independent of the direction of stretching.

Network analysis is performed using the NETWORKX package implemented in PYTHON [56]. When constructing the graph based on polymer network structures, crosslinkers of polymer networks are represented as nodes, and polymer chains are represented as edges. Primary loops in polymer networks, which are formed when both ends of a polymer strand are connected to the same crosslinker, are represented as self-loops. Secondary loops, formed when multiple polymer strands connect to the same pair of crosslinkers, are denoted as parallel edges between nodes. Higher-order cyclic defects, where order represents the number of polymer strands forming a cycle, are naturally incorporated into the graph [4]. Dangling ends are not included in the graphs. The sizes of graphs constructed in this way depend on the number of crosslinkers and polymer chains. Since the number of monomers is kept constant across different systems, systems with different strand lengths N will have graphs of different sizes. The influence of the sizes of the systems and the graphs on the results will be discussed.

The initial undeformed network structure is represented as an unweighted graph to calculate GEBC for all edges. GEBC of an edge e is defined as the sum of the fraction of all-pairs shortest paths that pass through it [26,56–58],

$$\text{GEBC}_e = \frac{2}{n(n-1)} \sum_{s,t} \frac{\sigma(s,t|e)}{\sigma(s,t)}, \tag{2}$$

where $\sigma(s,t)$ is the number of shortest paths between node s and t, and $\sigma(s,t|e)$ is the number of those paths that pass through e. Each GEBC value is normalized by $2/[n(n-1)]$ to restrict the value of GEBC to a range between 0 and 1. Additionally, following the approach employed in Berthier *et al.* [29], we further normalize GEBC by the average value of GEBC of all edges in the network to compare the relative importance of edges to others.

To investigate the geometric factor behind potential failure locations in polymer networks, the angle between each polymer strand and an axis α, θ_α is calculated based on the time-averaged positions of the crosslinkers attached to the polymer strand in the equilibrated network. The second Legendre polynomial is used to quantify the orientation of each polymer strand [59],

$$P_{2,\alpha}(\cos\theta_\alpha) = \tfrac{1}{2}(3\cos^2\theta_\alpha - 1), \tag{3}$$

where the $P_{2,\alpha}$ value is closer to 1 if the strand is more aligned with the axis α and is closer to $-1/2$ if the strand is more orthogonal to the axis α. We denote $P_{2,\text{loading}}$ as the value of P_2 calculated in the loading direction.

III. RESULTS AND DISCUSSION

We begin by demonstrating that the strands that fail during deformation are not a random subset of polymer strands. The distribution of P_{break} for polymer strands obtained from the isoconfigurational ensemble is compared with a random sampling test to determine whether the fracture of end-linked

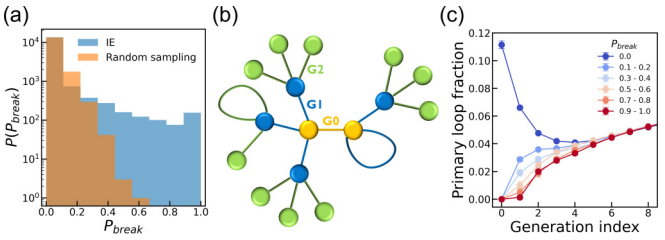

FIG. 1. For the $N = 5$ system, (a) distribution of probability of breaking (P_{break}) of polymer strands obtained from the isoconfigurational ensemble (blue) and the random sampling (orange); (b) schematic illustration showing the first three generations of the local structure of a polymer strand, with strands and crosslinkers at the same generation from the root (G0) strand labeled with the same color; (c) average primary loop fraction as a function of generation index for strands with different P_{break} in the isoconfigurational ensemble, zoomed in the low generation index region. The plot with the full range of values is available in the Supplemental Material [53].

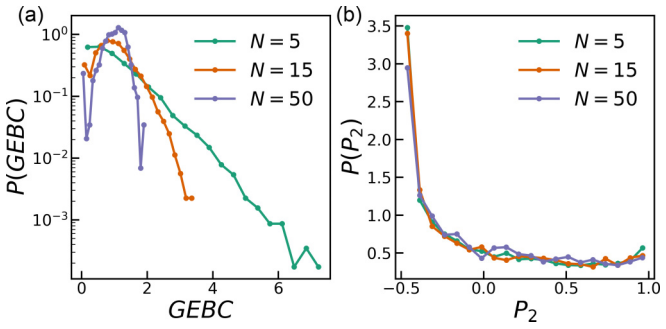

FIG. 2. Probability distribution function of (a) GEBC and (b) P_2 for the $N = 5$, 15, and 50 systems. GEBC and P_2 are calculated from the initial undeformed state of the network. GEBC of each polymer strand is normalized by the average value of all strands in the network.

polymer networks is a purely stochastic process. In each random sampling run, an equal number of broken strands as in each isoconfigurational ensemble run is randomly drawn. Blue histograms in Fig. 1(a) show the results from the isoconfigurational ensemble and orange histograms represent the results from the random sampling. The distribution of P_{break} between these two tests exhibits significant differences, with a distinct subset of polymer strands with very high P_{break} in the isoconfigurational ensemble. This finding suggests that the fracture process in polymer networks is not purely stochastic and is influenced by the network structure.

To explore the relationship between the network structure and the fracture behavior, we start with measuring the defect concentration in the local environment of each polymer strand. As depicted in Fig. 1(b), a polymer strand is chosen as the root (generation 0 strand), and other strands in the network can be located based on their topological distance (generation) from the root strand. For each polymer strand in the network, we can find its local environment and construct a subgraph including all strands within a certain range of generations of that strand. Then we group strands by their P_{break} obtained from the isoconfigurational ensemble and calculate the average primary loop fraction as a function of the generation index. The primary loop fraction represents the ratio of the number of primary loops to the total number of polymer strands in each subgraph. Figure 1(c) illustrates that for polymer strands with a finite P_{break}, the primary loop concentration in their local environment exhibits a significant difference compared to those strands that do not break in any run of the isoconfigurational ensemble. Moreover, for strands with high P_{break}, their local environment (the low generation index region) contains fewer primary loops compared to those with low P_{break}. The local environment analysis reveals that polymer strands with a relatively defect-free local structure are more susceptible to failure compared to those with a higher concentration of defects in their local surroundings. This observation aligns with the findings of Arora *et al.*, which reported that linear strands break prior to primary-loop-containing strands [12].

Mapping polymer networks to graphs and utilizing network analysis tools provide an alternative perspective for probing the structure of these complex disordered systems. The probability distribution functions of GEBC and P_2 of polymer strands, calculated from the initial undeformed state of networks, are shown in Fig. 2. While the shape of the distribution of P_2 is approximately constant across systems with different N, the shape of the distribution of GEBC varies. Through a finite-size effect analysis, we verify that this variation can be attributed to two reasons (see Supplemental Material [53] for details). First, networks with higher N at the same polymer mole fraction contain fewer loop defects [20,46], resulting in a more uniform distribution of GEBC compared to systems with lower N that have a higher defect concentration. Second, since the number of polymer beads is kept constant across systems with different N, the networks constructed will contain different numbers of polymer strands and crosslinkers, leading to graphs of varying sizes. Overall, the distribution of GEBC in all systems indicates that a small subset of polymer strands within the networks has GEBC values several times higher than the system average.

We proceed to group strands with the same P_{break} from the isoconfigurational ensemble together to investigate the underlying topological and geometric features of the network structure influencing the potential failure locations. Figure 3(a) demonstrates a consistent positive correlation between the average GEBC of each group and P_{break} across all systems, regardless of the shape of GEBC distribution in these systems. This indicates that in the end-linked network systems, on average, strands with higher GEBC have a higher probability of breaking. Moreover, Fig. 3(b) illustrates a positive correlation between average P_2 in the loading direction ($P_{2,\text{loading}}$) and P_{break}, as well as a negative correlation between average P_2 in the orthogonal directions and P_{break}. This finding suggests that strands that are more aligned with the loading direction have a higher probability of breaking. To further evaluate the effectiveness of GEBC and $P_{2,\text{loading}}$ on predicting the failure locations of end-linked polymer networks, we calculate the average P_{break} for polymer strands with GEBC and $P_{2,\text{loading}}$ above certain thresholds. As shown in Figs. 3(c) and 3(d), the average P_{break} increases as the GEBC and $P_{2,\text{loading}}$ threshold increase. In other words, polymer strands with higher GEBC and $P_{2,\text{loading}}$ generally have higher P_{break}, suggesting a bidirectional relationship between P_{break} and GEBC and $P_{2,\text{loading}}$. Furthermore, by plotting

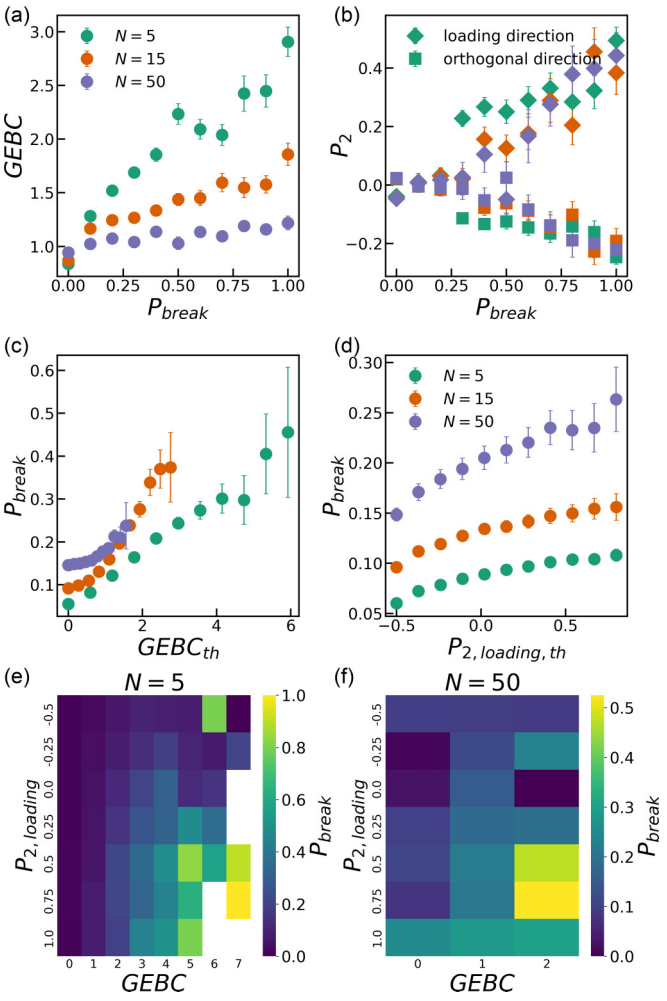

FIG. 3. For the $N = 5$, 15, and 50 network systems, average (a) GEBC and (b) P_2 for polymer strands with the same P_{break}. Average P_{break} for polymer strands that have (c) GEBC and (d) $P_{2,\text{loading}}$ above certain thresholds. Average P_{break} is also plotted as a function of both GEBC and $P_{2,\text{loading}}$ for the (e) $N = 5$ and (f) $N = 50$ systems.

average P_{break} as a function of both GEBC and $P_{2,\text{loading}}$, Figs. 3(e) and 3(f) reveal that polymer strands with both high GEBC and high $P_{2,\text{loading}}$ are more prone to break compared to those with lower GEBC and/or $P_{2,\text{loading}}$ values.

Average GEBC and $P_{2,\text{loading}}$ are also calculated as a function of the order in which the strands break during the deformation. Since the order in which the strands break can vary between each realization in the isoconfigurational ensemble, the average GEBC and $P_{2,\text{loading}}$ are calculated independently in each trajectory and plotted in Fig. 4. Both GEBC and $P_{2,\text{loading}}$ are highest for the first several chains that break then appear to decrease linearly as the deformation proceeds towards failure. In Fig. 4, the black lines in the plots represent linear fittings of these data points. The linear trend suggests that strand breaking events initiate from strands with higher GEBC and smaller angles between the polymer strands and the loading direction. We note that when the network approaches failure, GEBC approaches a value close to 1 and $P_{2,\text{loading}}$ decreases to approximately 0.0, which implies that the predicting power of these two factors diminishes as the network approaches the fracture point, but these measures are important in the initial stages of failure. These results also show the importance of topological and geometric features of the networks beyond the more common network defects such as loops and dangling ends.

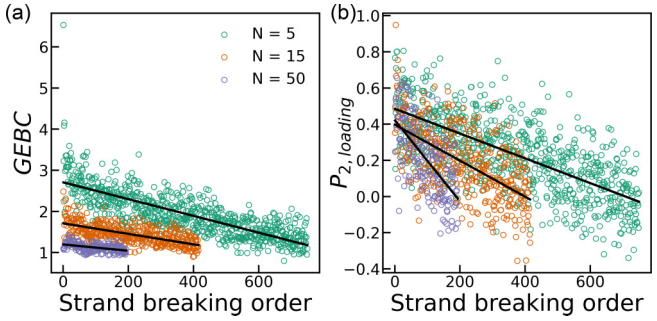

FIG. 4. Average (a) GEBC and (b) $P_{2,\text{loading}}$ as a function of the strand breaking order for the $N = 5$, 15, and 50 systems. Black lines are linear fittings of each data set.

IV. CONCLUSION

This work provides valuable insights into the interplay between network topology, strand orientation relative to the direction of strain, and the local failure behavior of model end-linked polymer networks. Through a combination of molecular simulations and network analysis techniques, we reveal that in the initial undeformed state of model end-linked polymer networks, polymer strands with relatively defect-free local structures, higher GEBC values, and greater alignment with the loading direction are more susceptible to failure during uniaxial tensile deformation. Additionally, strand breaking events initiate from polymer strands with higher GEBC values and smaller angles between the strand and the loading direction. The effectiveness of GEBC in identifying the failure locations at the strand level is consistent with recent observations in other types of network materials, including granular networks [29] and colloidal gels [35], highlighting the potential of network analysis tools in finding universal properties across different disordered network systems. Future work will explore the predictive capabilities of GEBC and strand orientation in other types of reaction schemes and deformation, as well as further investigate other network analysis techniques such as community detection [36]. These findings also offer a different perspective to understand the influence of topological defects in polymer networks and suggest a route to inversely design polymer network structures to control the location of fracture and achieve desired fracture properties.

ACKNOWLEDGMENTS

The authors thank Entao Yang for helpful discussion. The authors acknowledge support from the Office of Naval Research via ONR-N00014-17-1-2056. This work used Stampede2 at the Texas Advanced Computing Center (TACC) through allocation TG-DMR150034 from the Extreme Science and Engineering Discovery Environment (XSEDE)

program, which is supported by National Science Foundation Grant No. 1548562 and allocation CHM230005 from the Advanced Cyberinfrastructure Coordination Ecosystem: Services & Support (ACCESS) program, which is supported by National Science Foundation Grants No. 2138259, No. 2138286, No. 2138307, No. 2137603, and No. 2138296.

[1] J. A. Rogers, T. Someya, and Y. Huang, Materials and mechanics for stretchable electronics, Science **327**, 1603 (2010).

[2] L. Ionov, Hydrogel-based actuators: Possibilities and limitations, Mater. Today **17**, 494 (2014).

[3] J. Li and D. J. Mooney, Designing hydrogels for controlled drug delivery, Nat. Rev. Mater. **1**, 16071 (2016).

[4] Y. Gu, J. Zhao, and J. A. Johnson, Polymer networks: from plastics and gels to porous frameworks, Angew. Chem. Int. Ed. **59**, 5022 (2020).

[5] S. P. O. Danielsen, H. K. Beech, S. Wang, B. M. El-Zaatari, X. Wang, L. Sapir, T. Ouchi, Z. Wang, P. N. Johnson, Y. Hu, D. J. Lundberg, G. Stoychev, S. L. Craig, J. A. Johnson, J. A. Kalow, B. D. Olsen, and M. Rubinstein, Molecular characterization of polymer networks, Chem. Rev. **121**, 5042 (2021).

[6] X. Zhao, X. Chen, H. Yuk, S. Lin, X. Liu, and G. Parada, Soft materials by design: unconventional polymer networks give extreme properties, Chem. Rev. **121**, 4309 (2021).

[7] T. Zhou, H. Yuk, F. Hu, J. Wu, F. Tian, H. Roh, Z. Shen, G. Gu, J. Xu, B. Lu, and X. Zhao, 3D printable high-performance conducting polymer hydrogel for all-hydrogel bioelectronic interfaces, Nat. Mater. **22**, 895 (2023).

[8] E. Ducrot, Y. Chen, M. Bulters, R. P. Sijbesma, and C. Creton, Toughening elastomers with sacrificial bonds and watching them break, Science **344**, 186 (2014).

[9] S. Wang, S. Panyukov, M. Rubinstein, and S. L. Craig, Quantitative adjustment to the molecular energy parameter in the Lake-Thomas theory of polymer fracture energy, Macromolecules **52**, 2772 (2019).

[10] S. Lin and X. Zhao, Fracture of polymer networks with diverse topological defects, Phys. Rev. E **102**, 052503 (2020).

[11] A. Arora, T. S. Lin, H. K. Beech, H. Mochigase, R. Wang, and B. D. Olsen, Fracture of polymer networks containing topological defects, Macromolecules **53**, 7346 (2020).

[12] A. Arora, T. S. Lin, and B. D. Olsen, Coarse-grained simulations for fracture of polymer networks: stress versus topological inhomogeneities, Macromolecules **55**, 4 (2022).

[13] C. W. Barney, Z. Ye, I. Sacligil, K. R. McLeod, H. Zhang, G. N. Tew, R. A. Riggleman, and A. J. Crosby, Fracture of model end-linked networks, Proc. Natl. Acad. Sci. USA **119**, e2112389119 (2022).

[14] J. Tauber, J. van der Gucht, and S. Dussi, Stretchy and disordered: Toward understanding fracture in soft network materials via mesoscopic computer simulations, J. Chem. Phys. **156**, 160901 (2022).

[15] S. Wang, S. Panyukov, S. L. Craig, and M. Rubinstein, Contribution of unbroken strands to the fracture of polymer networks, Macromolecules **56**, 2309 (2023).

[16] B. Deng, S. Wang, C. Hartquist, and X. Zhao, Nonlocal intrinsic fracture energy of polymerlike networks, Phys. Rev. Lett. **131**, 228102 (2023).

[17] C. Creton, 50th anniversary perspective: networks and gels: soft but dynamic and tough, Macromolecules **50**, 8297 (2017).

[18] H. Zhou, J. Woo, A. M. Cok, M. Wang, B. D. Olsen, and J. A. Johnson, Counting primary loops in polymer gels, Proc. Natl. Acad. Sci. USA **109**, 19119 (2012).

[19] M. Zhong, R. Wang, K. Kawamoto, B. D. Olsen, and J. A. Johnson, Quantifying the impact of molecular defects on polymer network elasticity, Science **353**, 1264 (2016).

[20] R. Wang, A. Alexander-Katz, J. A. Johnson, and B. D. Olsen, Universal cyclic topology in polymer networks, Phys. Rev. Lett. **116**, 188302 (2016).

[21] M. Lang, Elasticity of phantom model networks with cyclic defects, ACS Macro Lett. **7**, 536 (2018).

[22] S. Panyukov, Loops in polymer networks, Macromolecules **52**, 4145 (2019).

[23] T. S. Lin, R. Wang, J. A. Johnson, and B. D. Olsen, Revisiting the elasticity theory for real Gaussian phantom networks, Macromolecules **52**, 1685 (2019).

[24] M. Rubinstein and R. H. Colby, in *Polymer Physics*, edited by R. H. Colby (Oxford University Press, Oxford, UK, 2003).

[25] G. J. Lake and A. G. Thomas, The strength of highly elastic materials, Proc. R. Soc. London, Ser. A **300**, 108 (1967).

[26] M. Newman, *Networks* (Oxford University Press, Oxford, UK, 2018).

[27] D. S. Bassett, E. T. Owens, K. E. Daniels, and M. A. Porter, Influence of network topology on sound propagation in granular materials, Phys. Rev. E **86**, 041306 (2012).

[28] L. Papadopoulos, M. A. Porter, K. E. Daniels, and D. S. Bassett, Network analysis of particles and grains, J. Complex Netw. **6**, 485 (2018).

[29] E. Berthier, M. A. Porter, and K. E. Daniels, Forecasting failure locations in 2-dimensional disordered lattices, Proc. Natl. Acad. Sci. USA **116**, 16742 (2019).

[30] J. E. Kollmer and K. E. Daniels, Betweenness centrality as predictor for forces in granular packings, Soft Matter **15**, 1793 (2019).

[31] Y. Yin, N. Bertin, Y. Wang, Z. Bao, and W. Cai, Topological origin of strain induced damage of multi-network elastomers by bond breaking, Extreme Mech. Lett. **40**, 100883 (2020).

[32] Y. Amamoto, K. Kojio, A. Takahara, Y. Masubuchi, and T. Ohnishi, Complex network representation of the structure-mechanical property relationships in elastomers with heterogeneous connectivity, Patterns **1**, 100135 (2020).

[33] M. Pournajar, M. Zaiser, and P. Moretti, Edge betweenness centrality as a failure predictor in network models of structurally disordered materials, Sci. Rep. **12**, 11814 (2022).

[34] M. Nabizadeh, A. Singh, and S. Jamali, Structure and dynamics of force clusters and networks in shear thickening suspensions, Phys. Rev. Lett. **129**, 068001 (2022).

[35] D. Mangal, M. Nabizadeh, and S. Jamali, Topological origins of yielding in short-ranged weakly attractive colloidal gels, J. Chem. Phys. **158**, 014903 (2023).

[36] F. Fazelpour, V. D. Desai, and K. E. Daniels, Community detection forecasts material failure in a sheared granular material, arXiv:2307.07501.

[37] P. Moretti and M. Zaiser, Network analysis predicts failure of materials and structures, Proc. Natl. Acad. Sci. USA **116**, 16666 (2019).

[38] L. C. Freeman, A set of measures of centrality based on betweenness, Sociometry **40**, 35 (1977).

[39] G. S. Grest, K. Kremer, and E. R. Duering, Kinetics of end crosslinking in dense polymer melts, Europhys. Lett. **19**, 195 (1992).

[40] E. R. Duering, K. Kremer, and G. S. Grest, Structure and relaxation of end-linked polymer networks, J. Chem. Phys. **101**, 8169 (1994).

[41] C. Nowak and F. A. Escobedo, Tuning the sawtooth tensile response and toughness of multiblock copolymer diamond networks, Macromolecules **49**, 6711 (2016).

[42] C. Nowak and F. A. Escobedo, Optimizing the network topology of block copolymer liquid crystal elastomers for enhanced extensibility and toughness, Phys. Rev. Mater. **1**, 035601 (2017).

[43] A. A. Gusev, Numerical estimates of the topological effects in the elasticity of Gaussian polymer networks and their exact theoretical description, Macromolecules **52**, 3244 (2019).

[44] M. Lang and T. Müller, Analysis of the gel point of polymer model networks by computer simulations, Macromolecules **53**, 498 (2020).

[45] Z. Ye and R. A. Riggleman, Molecular view of cavitation in model-solvated polymer networks, Macromolecules **53**, 7825 (2020).

[46] H. Zhang and R. A. Riggleman, Percolation of co-continuous domains in tapered copolymer networks, Mol. Syst. Des. Eng. **8**, 115 (2023).

[47] Y. Masubuchi, Y. Doi, T. Ishida, N. Sakumichi, T. Sakai, K. Mayumi, and T. Uneyama, Phantom chain simulations for the fracture of energy-minimized tetra- and tri-branched networks, Macromolecules **56**, 2217 (2023).

[48] V. Sorichetti, A. Ninarello, J. Ruiz-Franco, V. Hugouvieux, E. Zaccarelli, C. Micheletti, W. Kob, and L. Rovigatti, Structure and elasticity of model disordered, polydisperse, and defect-free polymer networks, J. Chem. Phys. **158**, 074905 (2023).

[49] S. Plimpton, Fast parallel algorithms for short-range molecular dynamics, J. Comput. Phys. **117**, 1 (1995).

[50] A. P. Thompson, H. M. Aktulga, R. Berger, D. S. Bolintineanu, W. M. Brown, P. S. Crozier, P. J. in 't Veld, A. Kohlmeyer, S. G. Moore, T. D. Nguyen, R. Shan, M. J. Stevens, J. Tranchida, C. Trott, and S. J. Plimpton, LAMMPS - a flexible simulation tool for particle-based materials modeling at the atomic, meso, and continuum scales, Comput. Phys. Commun. **271**, 108171 (2022).

[51] T. J. Boerner, S. Deems, T. R. Furlani, S. L. Knuth, and J. Towns, ACCESS: Advancing Innovation: NSF's Advanced Cyberinfrastructure Coordination Ecosystem: Services & Support, in *Practice and Experience in Advanced Research Computing*, (ACM, New York, 2023), pp. 173–176.

[52] C. N. Walker, K. C. Bryson, R. C. Hayward, and G. N. Tew, Wide bicontinuous compositional windows from co-networks made with telechelic macromonomers, ACS Nano **8**, 12376 (2014).

[53] See Supplemental Material at http://link.aps.org/supplemental/10.1103/PhysRevMaterials.8.035604 for molecular dynamics simulation details, sample stress-strain curves, full plot of primary loop fraction as a function of generation index, and finite-size effect analysis, which includes Refs. [13,20,45,46,49,50,52,60–62].

[54] A. Widmer-Cooper, P. Harrowell, and H. Fynewever, How reproducible are dynamic heterogeneities in a supercooled liquid? Phys. Rev. Lett. **93**, 135701 (2004).

[55] J. Colombo, A. Widmer-Cooper, and E. Del Gado, Microscopic picture of cooperative processes in restructuring gel networks, Phys. Rev. Lett. **110**, 198301 (2013).

[56] A. A. Hagberg, D. A. Schult, and P. J. Swart, in *Proceedings of the 7th Python in Science Conference*, edited by G. Varoquaux, T. Vaught, and J. Millman (Pasadena, CA, 2008), pp. 11–15, https://conference.scipy.org/proceedings/scipy2008/paper_2/.

[57] U. Brandes, A faster algorithm for betweenness centrality, J. Math. Sociol. **25**, 163 (2001).

[58] U. Brandes, On variants of shortest-path betweenness centrality and their generic computation, Soc. Netw. **30**, 136 (2008).

[59] P. G. de Gennes and J. Prost, *The Physics of Liquid Crystals* (Clarendon Press, Oxford, UK, 1993).

[60] R. Auhl, R. Everaers, G. S. Grest, K. Kremer, and S. J. Plimpton, Equilibration of long chain polymer melts in computer simulations, J. Chem. Phys. **119**, 12718 (2003).

[61] Y. R. Sliozberg and J. W. Andzelm, Fast protocol for equilibration of entangled and branched polymer chains, Chem. Phys. Lett. **523**, 139 (2012).

[62] T. Ge, F. Pierce, D. Perahia, G. S. Grest, and M. O. Robbins, Molecular dynamics simulations of polymer welding: Strength from interfacial entanglements, Phys. Rev. Lett. **110**, 098301 (2013).